International Journal of Energy Production and Management
https://www.acadlore.com/journals/IJEPM

The Solar Tower Chimney Geometry Impact on Its Performance

Leridi Nadia[1*], Oussama Benbouaziz[2], Zeroual Aouachria[1]

[1] Applied Energy Physics Laboratory, Department of Physics, University of Batna 1 (Hadj Lakhdar), 05000 Batna, Algeria
[2] École Nationale Polytechnique de Constantine, BP 75-25000 Constantine, Algeria

[*] Correspondence: Leridi Nadia (nadia.leridi@univ-batna.dz)

Received: 10-16-2025 **Revised:** 11-15-2025 **Accepted:** 12-18-2025

Citation: L. Nadia, O. Benbouaziz, and Z. Aouachria, "The solar tower chimney geometry impact on its performance," *Int. J. Energy Prod. Manag.*, vol. 10, no. 4, pp. 766–784, 2025. https://doi.org/10.56578/ijepm100414.

Abstract: In this study, the effect of the collector-chimney junction geometry on the performance of a Solar Chimney Power Plant (SCPP) is investigated using numerical simulations based on a two-dimensional axisymmetric model with the standard k-ε turbulence model, coupled with the Discrete Ordinates (DO) radiation model. An SCPP with a collector diameter of 3 m and a chimney height of 3 m is considered. Several junction configurations are analyzed by varying the junction inclination angle, arc radius, and fillet radius. The results show that the junction configuration with a collector inclination angle of 20° and a fillet radius of 14 cm provides the best performance among the inclined cases, enhancing the mass flow rate by approximately 3.2% and increasing the power density by about 15% compared to the same inclination angle without a fillet. In addition, the configuration incorporating an 18 cm arc radius combined with a 14 cm fillet radius increases the mass flow rate by around 1.7% and improves the power density by approximately 7.5% compared to the corresponding arc configuration without a fillet Furthermore, a comparative analysis between configurations with and without a fillet radius reveals that the introduction of a fillet significantly improves the overall system performance, yielding increases of up to 8% in mass flow rate and about 5% in power density. These enhancements are attributed to smoother airflow transitions and more efficient inlet acceleration at the collector-chimney junction, leading primarily to improved aerodynamic performance of the solar chimney system.

Keywords: Solar energy; Solar chimney; Power plant; Collector-chimney junction; CFD; Power output

1 Introduction

Solar energy has emerged as one of the most widespread and reliable forms of renewable energy due to its availability and environmental compatibility. Numerous technologies have been developed to harness this resource and convert it into electricity. Among these technologies, Solar Chimney Power Plant (SCPP) represent a promising solution, particularly in regions characterized by high levels of high solar irradiation throughout the day. These systems enable the efficient utilization of large land areas to generate electricity in a safe, sustainable, and emission-free manner. Since the demonstration of the first solar chimney prototype in Spain by engineers Haaf et al. [1], this concept has attracted increasing interest from researchers community.

Numerous studies have been conducted to assess the performance of the solar chimneys and evaluate their energy generation capacity and operational efficiency. Other investigations have focused on identifying system limitations and challenges related to practical implementation. To enhance the energy efficiency of SCPP, various optimization strategies have been proposed. In particular, the Manzanares prototype has been widely used as a reference to assess the viability of the concept in arid desert climates. Rabehi et al. [2] employed CFD simulations to evaluate SCPP performance across four Algerian regions, incorporating meteorological parameters such as solar radiation and ambient temperature. Their results indicated an average monthly output of 68 to73 kW, with an hourly peak of 113 kW in June in Tamanrasset. Sellami et al. [3] analyzed the Manzanares prototype applied to Tamanrasset and Constantine, demonstrating that secondary or tertiary collector roofs could achieve annual outputs of 51 to 79 kW, with hourly peaks of 80 kW in June. Collectively, these studies highlight not only the technological feasibility of SCPP in arid regions such as southern Algeria but also their potential for optimization and dynamic adaptation to local energy demand.

Recent research on SCPP demonstrates a growing interest in hybrid configurations, aiming to overcome the inherent limitations of purely solar systems. Indeed, this technology still suffers from low energy efficiencies and intermittent operation due to its direct dependence on solar radiation. Faced with these constraints, several authors, including Al-Kayiem et al. [4] performed a CFD-based aerodynamic and thermodynamic analysis of a hybrid solar chimney integrated with a gas turbine to recover exhaust heat for continuous operation. The results showed a notable rise in power output (49.04 kW to 67 kW) and collector efficiency (34.3 % to 78.5 %), demonstrating that exhaust gas heat recovery greatly enhances the energy efficiency and stability of the hybrid system. Habibollahzadea et al. [5] proposed combining a SCPP with a waste-to-energy (WTE) unit to improve electricity production at night. In this system, hot air from the WTE unit is injected into the chimney, which increases the power output. Singh et al. [6] investigated the integration of photovoltaic (PV) panels into a hybrid solar chimney power plant (HSCPP). Their results showed that using a converging collector and a diverging chimney enhanced PV efficiency by approximately 7 %, with passive PV cooling proving particularly effective over 80 % of the collector surface. More recently, Pandey et al. [7] analyzed the performance of a solar chimney integrated with a subsurface heat exchanger (HE) designed to recover residual ground heat and enable nighttime power generation. Their results showed that this concept can extend chimney operation after sunset and improve the stability of electricity supply. Mohammed et al. [8] studied a HSCPP incorporating phase-change materials (PCM) in the collector and modified with a cavity structure to improve heat storage and distribution. Using three-dimensional CFD modeling, the authors showed that adding PCM to the collector increases the air temperature by nearly 20 % and the power output by approximately 25 % compared to the conventional model. Furthermore, the cavity structure optimizes heat flow and extends system operation after sunset. Azad et al. [9] conducted a multi-objective optimization of a solar chimney system integrated with electricity-generation and water desalination, by combining CFD simulations with artificial neural networks (ANN), they predicted collector temperature and turbine velocity based on geometric parameters. Results showed that the optimized geometry increased system efficiency by over 20 % and improved desalination output. Fadaei et al. [10] studied a HSCPP incorporating PCM in the collector to store and release thermal energy. Using ANN, they accurately predicted key performance indicators such as air velocity, outlet temperature, and power output, with correlation coefficients greater than 0.99. The integration of PCM improved thermal stability and enabled extended operation into the night.

Due to the high cost of building and operating hybrid systems, the exploration of numerous configurations is limited. Consequently, researchers have concentrated on geometric optimization to maximize energy performance while keeping costs manageable. To date, most studies have primarily addressed the technical aspects of SCPP. Mandal et al. [11] used ANN to analyze the effect of geometric parameters (chimney height, air inlet diameter, collector area) on the performance of a solar power plant with a chimney. Using CFD data, their model predicted performance with over 98% accuracy. The results indicate that a greater chimney height and a larger collector area improve mass flow rate and power density, while an excessively large inlet diameter reduces efficiency. The study confirms the effectiveness of AI for the geometric optimization of solar power plants with chimneys. Abdul Hussein et al. [12] investigated a solar chimney system incorporating geometric modifications to the nozzle and canopy to optimize performance. Using CFD modeling, they demonstrated that adding a convergent nozzle and an optimized canopy increased the updraft velocity to 17.8 m/s (compared to 16.0 m/s for the conventional SCPP) and the power output to 67 kW (from 49 kW), significantly enhancing the system's aerodynamic and energy efficiency. Cuce et al. [13] studied the effect of chimney height on the therm-aerodynamic performance of the Manzanares prototype, showing that greater height improves power output up to a threshold where pressure losses and structural stresses reduce additional gains. Subsequently, in their more recent work [14], the authors combined CFD modeling and ANN to analyze the impact of system geometry on the efficiency of SCPP. They demonstrated that a chimney divergence close to 2° and a collector angle between 5° and 7° promote an increase in air velocity, pressure gradient, and power generated, surpassing conventional cylindrical designs.

Ghernaout et al. [15] conducted a parametric CFD study on the airflow structure in a SCPP to evaluate the effect of geometric and thermal parameters on its performance. The authors showed that increasing the chimney radius and the temperature of the absorbing soil increases the upward air velocity by approximately 20 % and the power density by nearly 18 %. Conversely, certain configurations cause recirculation zones that reduce efficiency. Kasaeian et al. [16] and Ghalamchi et al. [17] conducted experimental and numerical investigations using a scaled prototype at the University of Tehran to optimize the geometric parameters of solar chimneys. Their results demonstrated that reducing the collector inlet height, increasing chimney height, and employing high thermal conductivity materials such as aluminum significantly enhanced thermal performance. Furthermore, Mandal et al. [18] introduced an innovative absorber surface design in which the conventional flat surface was replaced with a wavy triangular profile; their analysis confirmed improvements in both energy output and efficiency. Singh et al. [19] performed a numerical analysis of a divergent SCPP configuration that included an arc and fillet radius at the chimney base, resulting in enhanced airflow uniformity and increased power output. Mandal et al. [20] investigated the effects of chimney divergence and collector inclination on the performance of solar chimney power plants. Their findings indicate

that these parameters significantly enhance thermal efficiency and energy output by optimizing airflow and solar radiation absorption. Singh and Kumar [21] introduced a technical innovation by incorporating a bell-mouth inlet into a convergent-divergent solar chimney system. CFD simulations revealed an approximately 270 % increase in air velocity and an electricity output of up to 1,738 kW compared to conventional designs.

The performance of solar chimney power plants depends on several key design parameters, including the chimney height, collector geometry, and collector area. According to the existing literature, most previous studies have primarily focused on these global geometric parameters because of their direct influence on airflow behavior, heat transfer, and overall energy efficiency. However, the geometry of the collector-chimney junction has received relatively little attention, even though it represents a critical transition zone where complex flow phenomena occur. This research gap highlights the need for a more comprehensive investigation into how junction configuration affects the overall performance of solar chimney systems.

In this context, the present study focuses on the structural optimization of the collector-chimney junction. Targeted geometric modifications to the collector-chimney connection are proposed (Table 1) with the aim of enhancing flow stability, aerodynamic performance, and overall energy conversion efficiency.

Table 1. Variable dimensions of the chimney base

Parameter	Index	Size
Collector with inclination angle	θ_{Col}	10–30°
Collector with arc	R_{Ac}	6–18 cm
Chimney base with fillet	R_{fillet}	8–14 cm

2 Physical Model

Figure 1 shows schematic illustration of the operating principle of a SCPP. Ambient air is heated beneath the solar collector (transparent cover), creating a density gradient that induces an upward airflow through the vertical chimney. This airflow is exploited by a wind turbine installed at the chimney base to convert kinetic energy into electricity [22].

In this study, the geometric dimensions of the solar chimney were adopted from the experimental setup of Ghalamchi et al. [17] to ensure accurate validation of the proposed numerical model. A two-dimensional CFD model is developed using ANSYS Design Modeler, as illustrated in Figure 1, which presents the configuration of the conventional solar chimney system together with the applied boundary conditions (Table 2).

The proposed geometric configurations are illustrated, highlighting the modifications at the junction between the collector outlet and the chimney inlet

Figure 2 illustrate variations in the collector inclination angle (10°–30°) and the arc-shaped junction with radius ranging from 6 to 18 cm, respectively. Figures 3 present the combined configurations, incorporating a curved chimney base (fillet) with radius varying from 8 to 14 cm.

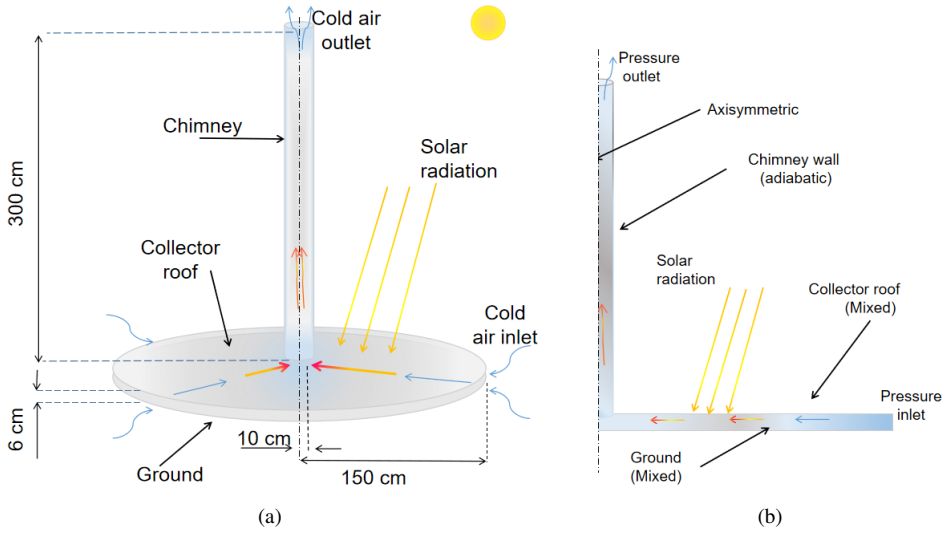

Figure 1. Structural of conventional solar chimney power plants (SCPP)

Table 2. Boundary conditions for ANSYS Fluent model

Collector Roof	Mixed, h = 10 w / m^2	Wall (Semi Transparant)
Ground	Mixed, h = 10 w / m^2	Wall (opaque)
Chimney	Adiabatic (Heat flux = 0)	Wall (opaque)
Collector inlet	Tamb = 300 k, Pgauge = 0 Pa	Pressure inlet
Chimney outlet	Pgauge = 0 Pa	Pressure outlet

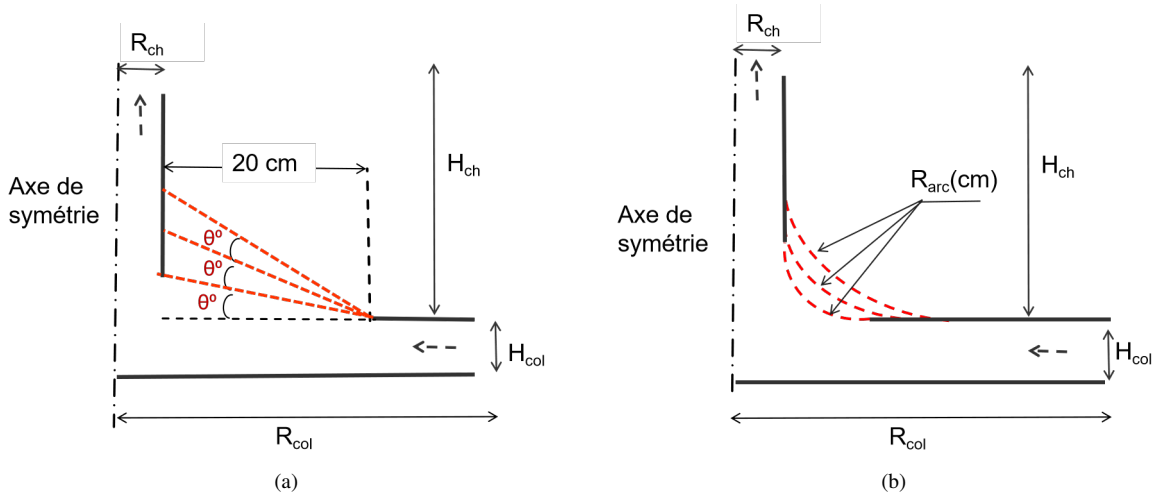

Figure 2. Chimney base configurations with different collector angles and arc radius

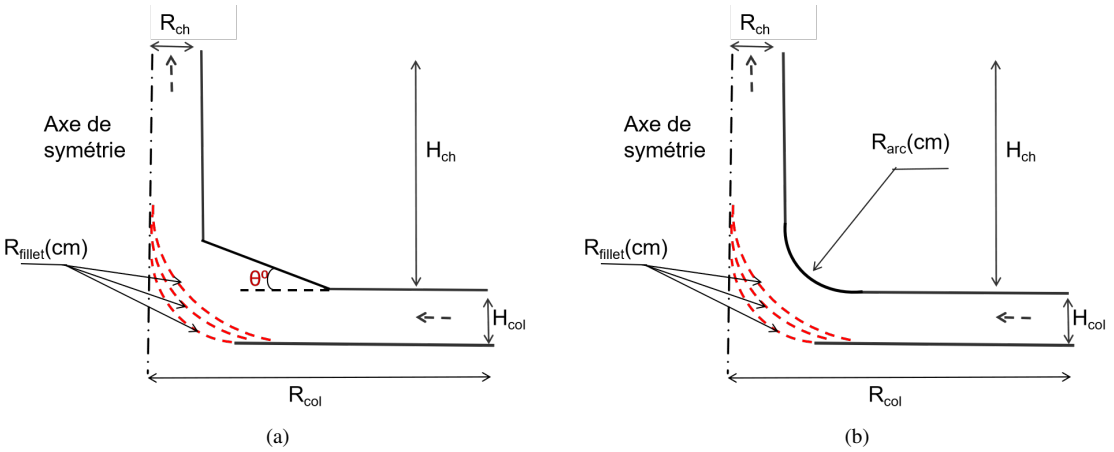

Figure 3. Chimney base configurations with varying fillet radius

2.1 Mathematical Formulation and Modelling

Following the assumptions reported by Kaplan [23], the flow within the solar chimney system is modeled as a two-dimensional, axisymmetric problem. The governing equations include the continuity equation, the momentum equations, and the energy equation, as detailed by Mirzamohammad et al. [24].

$$\frac{\partial(\rho u)}{\partial x} + \frac{\partial(\rho v)}{\partial y} = 0 \tag{1}$$

$$\frac{\partial(\rho u)}{\partial t} + \frac{\partial(\rho uu)}{\partial x} + \frac{\partial(\rho vu)}{\partial y} = -\frac{\partial p}{\partial x} + \mu\left[\frac{\partial^2 u}{\partial x^2} + \frac{\partial^2 u}{\partial y^2}\right] + \rho g_x \beta \Delta T \tag{2}$$

$$\frac{\partial(\rho v)}{\partial t} + \frac{\partial(\rho uv)}{\partial x} + \frac{\partial(\rho vv)}{\partial y} = -\frac{\partial p}{\partial y} + \left[\frac{\partial^2 v}{\partial x^2} + \frac{\partial^2 v}{\partial y^2}\right] \tag{3}$$

$$\rho c_p \left(\frac{\partial T}{\partial t} + u\frac{\partial T}{\partial x} + v\frac{\partial T}{\partial y} \right) = k \left(\frac{\partial^2 T}{\partial^2} + \frac{\partial^2 T}{\partial^2} \right) + S_T \tag{4}$$

where, u and v (m/s), are the velocity components in the x and y directions, respectively, and ΔT (K) represents the temperature difference between the air inside the chimney and the ambient air.

In this study, the standard k-ε turbulence model is adopted due to its proven robustness and computational efficiency in mixed convection flows, as well as its extensive validation in solar chimney configurations [16, 25, 26]. Although the RNG and realizable k-ε variants may provide improved predictions for strongly swirling or highly anisotropic flows, the standard model offers an optimal balance between accuracy, numerical stability, and computational cost. This choice is consistent with recent numerical investigations on solar chimneys, including the work of Ayadi et al. [26].

$$\frac{\partial}{\partial t}(\rho k) + \frac{\partial}{\partial x}(\rho u k) + \frac{\partial}{\partial y}(\rho v k) = \left(\mu + \frac{\mu_t}{\sigma_k} \right) \left(\frac{\partial^2 k}{\partial x^2} + \frac{\partial^2 k}{\partial y^2} \right) + \rho G_K + G_b - \rho\varepsilon \tag{5}$$

$$\frac{\partial}{\partial t}(\rho\varepsilon) + \frac{\partial}{\partial x}(\rho u\varepsilon) + \frac{\partial}{\partial y}(\rho v\varepsilon) = \left(\mu + \frac{\mu_t}{\sigma_\varepsilon} \right) \left(\frac{\partial^2 \varepsilon}{\partial x^2} + \frac{\partial^2 \varepsilon}{\partial y^2} \right) + \frac{\varepsilon}{k} C_1 \left(\rho G_k + C_3 G_b \right) - C_2 \rho \frac{\varepsilon^2}{k} \tag{6}$$

where, G_k represents the generation of turbulent kinetic energy due to gradients of the mean velocity. G_b denotes the generation of turbulent kinetic energy due to buoyancy effects. The model constants have the following values: $C_1 = 1.44, C_2 = 1.92, \sigma_k = 1.0, \sigma_\varepsilon = 1.3$.

Regarding irradiation heat transfer, the Discrete Ordinates (DO) model available in ANSYS Fluent is employed. This model is based on the numerical solution of the radiative transfer equation in participating and semi-transparent media, such as the glass cover of the solar collector considered in the present study. The DO approach is particularly suitable due to its ability to accurately capture directional radiation effects and radiation–matter interactions [11].

$$\nabla \cdot \left(I(\vec{r}, \vec{s})\vec{s} \right) + (a + \sigma_s)\, I(\vec{r}, \vec{s}) = an^2 \frac{\sigma T^4}{\pi} + \frac{\sigma_s}{4\pi} \int_0^{4\pi} I\left(\vec{r}, \vec{s}'\right) \omega\left(\vec{s}, \vec{s}'\right) d\Omega' \tag{7}$$

The Boussinesq approximation was used to calculate the density variation [27].

$$\rho - \rho_0 = -\rho_0 \beta \left(T - T_0 \right) \tag{8}$$

2.2 Modeling the Performance of SCPP

In order to objectively compare the efficiency of the investigated configurations, the potential aerodynamic power at the system outlet is evaluated without considering the presence of a wind turbine. This assumption ensures a fair assessment of the impact of geometric modifications. Under this framework, the air mass flow rate is determined using the following expression [28].

$$\dot{m} = \rho v_{Chimneymax} A_{Chimney} \tag{9}$$

The chimney efficiency [29] is given by Eq. (10)

$$\eta_{Chimney} = \frac{P_{tot}}{\dot{Q}} = \frac{gH_{Chimney}}{cpT_a} \tag{10}$$

In the absence of a wind turbine, the airflow reaches its maximum velocity, and the entire pressure difference across the system is utilized to accelerate the air, thereby converting it into kinetic energy [30]. Under these conditions, the theoretical power output of the system can be reasonably estimated using the updraft power density concept [19].

$$P = \frac{1}{2}\rho v^3 Chimneymax \tag{11}$$

Inside the chimney, the maximum air velocity [31].

$$v = \sqrt{2gH_{Chimney}\frac{\Delta T}{T_a}} \tag{12}$$

The convective heat transfer coefficient (h) represents the rate of heat exchange between the air inside the collector and the transparent cover. In solar chimney studies, h typically ranges from 5 to 12 W/m^2.K, based on experimental and numerical results [32].

In the present work, a value of W/m^2.K is adopted, consistent with the literature Rabehi et al. [2]. A constant solar irradiation of 850 W/m^2 is assumed, following previous studies on solar chimney power plants [3, 19, 21]. This benchmark value enables a direct comparison of results and facilitates the analysis of peak system performance.

The computational domain is divided into three distinct regions: The collector, the junction, and the chimney. A structured mesh conforming to the geometry of each region was generated using ANSYS. The pressure-velocity coupling is achieved through the SIMPLE method, while gradients are computed using the Green-Gauss cell-based approach. Pressure discretization is performed with a second-order scheme, and the momentum and energy equations are solved using a second-order upwind scheme. For the turbulence and the DO equations, a first-order discretization scheme is employed.

2.3 Mesh Independence and Validation

To assess the influence of mesh resolution on the numerical results, three different meshes were compared: a coarse mesh with 13,300 elements, a medium mesh with 19,300 elements, and a fine mesh with 26,200 elements. As shown in Figure 4, the differences in chimney exit velocity between the medium and fine meshes was less than 2%. This analysis confirmed that the medium mesh offered the best balance between accuracy and computational cost.

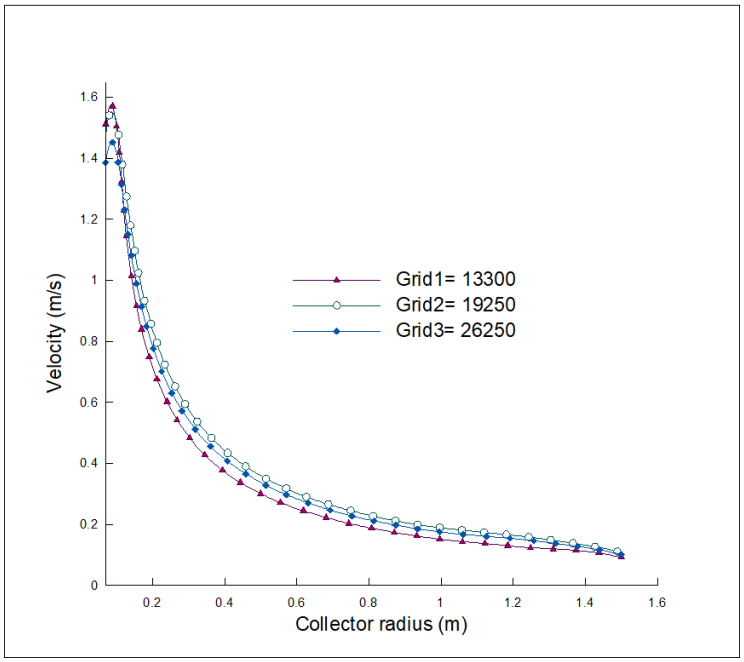

Figure 4. Grid independence for the conventional solar chimney design

To validate the numerical model, the simulation results were compared with reference experimental data [17]. The dimensions and boundary conditions were kept identical to those of the experimental setup. The prototype geometry has a horizontal solar radiation absorption surface with a radius of 3 m, a solar collector inlet height of 6 cm, a chimney height of 3 m, and a chimney diameter of 10 cm. The standard k-ε turbulence model with wall-function treatment was employed, and the near-wall mesh resolution was verified. The dimensionless wall distance falls within the range $0.54 < Y + < 11.94$ which is consistent with the recommended values for the standard k-ε model and ensures an appropriate representation of the near-wall boundary-layer behavior.

Figure 5 presents the velocity and temperature profiles, showing that the numerical simulation closely follows the experimental trends. The peak velocity 1.55 m/s occurs near the chimney axis (0.1 m from the inlet) and decreases toward the collector entrance. A minor deviation is observed near the inlet, where the simulated peak velocity is 1.40 m/s compared to the experimental value of 1.55 m/s, corresponding to a relative error of 9.6%. Similarly, the temperature profile exhibits a maximum of 329 K at the chimney center, decreasing radially toward the ambient temperature of 305 K. The simulation successfully reproduces this behavior, with a slight deviation at 0.1 m from the inlet, where the predicted temperature is 326 K compared to the experimental value of 329 K, resulting in a relative error of 0.9%. Overall, despite localized differences, the Standard k-ε model accurately predicts the dominant flow and thermal characteristics, confirming its suitability for the present study.

The thermal and physical properties of the key components of the SCPP studied here are summarized in Table 3 and evaluated at ambient conditions. All values are obtained from experimental measurements and validated literature sources, ensuring consistency and accuracy in the CFD simulations [30].

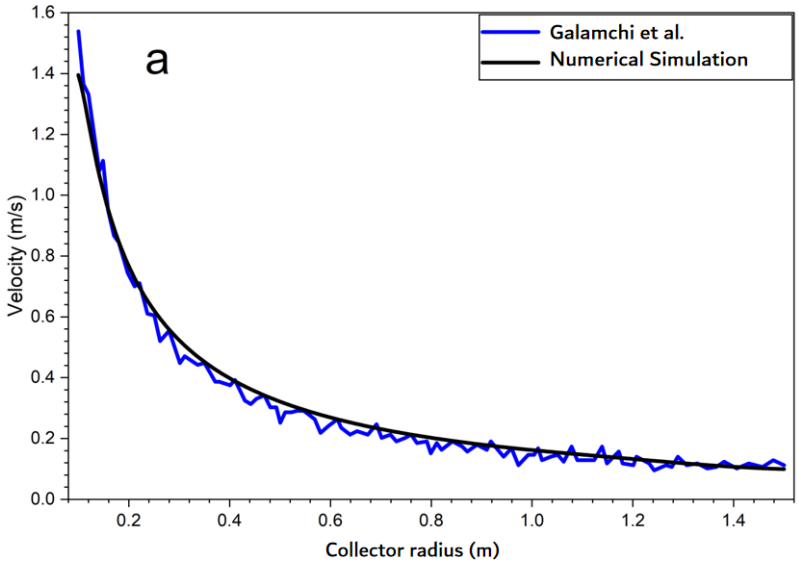

(a)

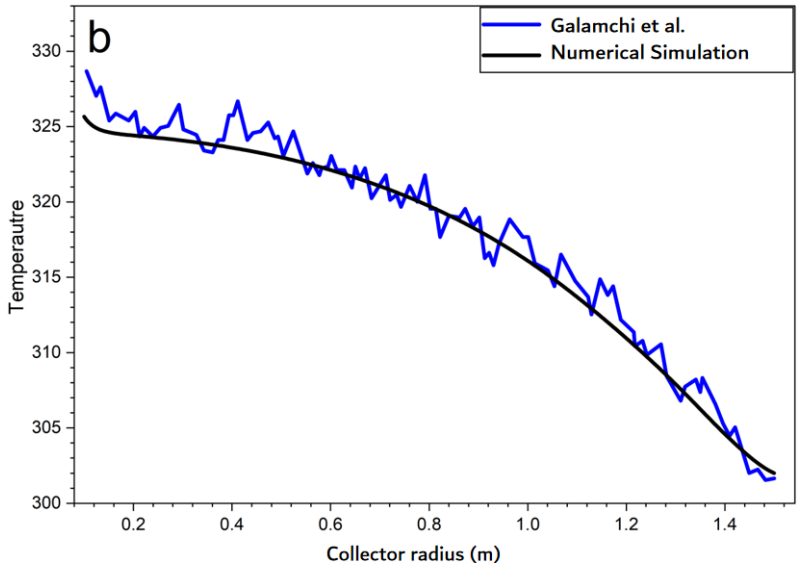

(b)

Figure 5. Validation of numerical and experimental data [17] for the conventional model

Table 3. Thermal and physical properties of solar chimney power plants (SCPP) components at ambient conditions [30]

Property / Material	Collector	Ground	Chimney	Units
Density	2500	2160	2719	(kg/m^3)
Thermal conductivity	1.15	1.83	202.4	(W/mK)
Specific heat	750	710	871	(J/kgK)
Absorption coefficient	0.03	0.9	0	-
Transmissivity	0.9	Opaque	Opaque	-
Emissivity	0.1	0.9	1	-
Refractive index	1.526	1	1	-

3 Results and Discussion

This section presents in detail how the shape of the chimney base geometry influences the performance and behaviour of airflow and heat transfer within the SCPP. Four distinct geometric configurations are considered in the

analysis. The simulation was conducted for various collector inclination angles (10°, 15°, 20°, 25°, and 30°) and arc radius (6 cm, 8 cm, 12 cm, and 18 cm).

First, a comparison was made between two approaches: gradually increasing the collector inclination angle and widening the radius of curvature of the junction between the collector outlet and the chimney inlet, while maintaining the conventional geometry of the chimney base.

Second, the same comparison was repeated, varying the fillet radius of the chimney base using different fillet radii. The results obtained for the various configurations are presented and discussed in the following sections.

3.1 Comparison between the effect of the inclination angle and the collector arc on the flow

In a conventional solar chimney system, the chimney is designed as a vertical cylinder positioned perpendicular to the horizontal solar collector in order to generate an upward airflow, The objective of this study is to compare the effects of the collector inclination angle and the arc radius while maintaining a conventional chimney base geometry as shown in Figure 2.

3.1.1 Influence of geometry on the air velocity

Figure 6 illustrate the velocity distribution along the chimney height for different collector–chimney junction geometries. For the inclined collector configuration, relatively high inlet velocities are observed, reaching a maximum value of 1.23 m/s at the chimney inlet. This maximum velocity fully justifies the choice of locating the turbine at this position to take advantage of the more active airflow. In comparison, the arc-shaped collector configuration promotes a smoother acceleration of the airflow starting from the collector outlet. This geometry leads to a more uniform velocity distribution along the chimney height. For an arc radius of 18 cm, the inlet velocity reaches a maximum value of approximately 1.21 m/s. Although this peak velocity is slightly lower than that obtained with the inclined configuration, the arc-shaped configuration provides a more stable and evenly distributed airflow, which is favorable for system efficiency.

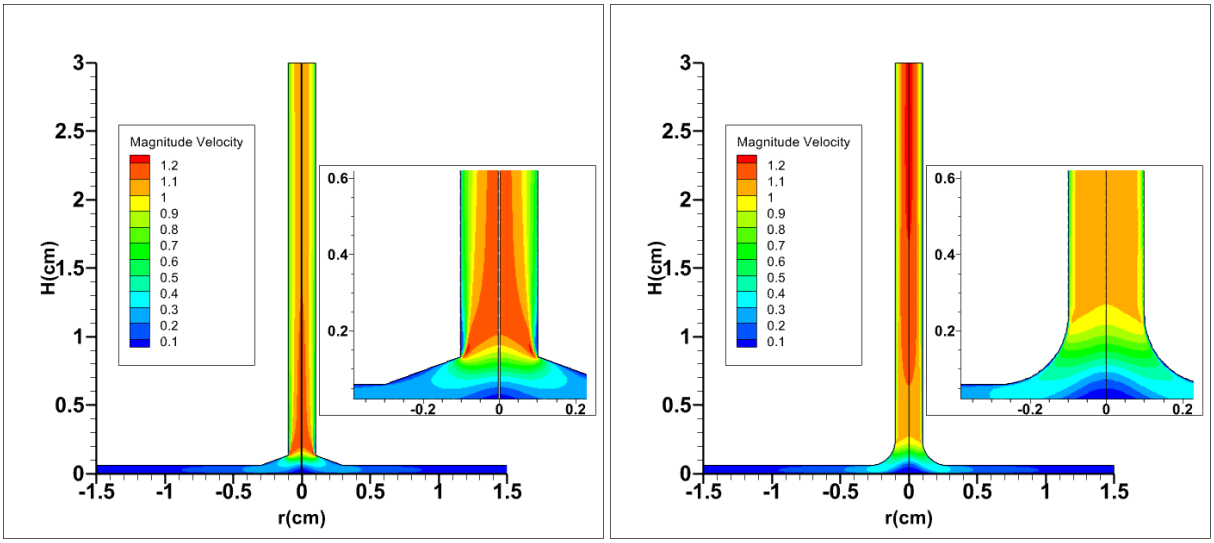

(a) Inclination angle θ = 20°

(b) With an arc radius = 18 cm

Figure 6. Velocity contours for a solar chimney power plants (SCPP) with a conventional chimney base

As shown in Figure 7, the velocity profiles exhibit a generally similar trend across all configurations, characterized by a gradual increase in velocity from the collector inlet. This similarity persists up to the point where the collector geometry begins to vary (at approximately 130 cm). These findings highlight the significant influence of the collector-chimney junction geometry on the velocity distribution within the system.

The inclination of the collector has a significant impact on the aerodynamic performance of the system. For low inclination angles (0°–10°), the airflow acceleration is enhanced, indicating a more effective thermal updraft. However, when the inclination angle exceeds 20°, a noticeable reduction in velocity occurs, suggesting increased flow disturbance and a degradation of aerodynamic performance.

Configurations with smaller arc radius (6–8 cm) promote greater heat concentration and consequently higher airflow velocity. In contrast, increasing the arc height (12–18 cm) results in flow expansion and a reduction in the average velocity, indicating a loss of available kinetic energy.

Excluding the conventional configuration ($\theta = 0°$), the collector geometry with an arc radius of 6 cm exhibits the highest average chimney outlet velocity, reaching approximately 0.55 m/s, compared to 0.36 m/s for the configuration with a 10° inclined collector. This represents an improvement of about 53%, calculated according to:

$$\text{Improvement } (\%) = \frac{V_{\text{arc6cm}} - V_{10°}}{V_{10°}} \times 100 = \frac{0.55 - 0.36}{0.36} \approx 53\% \tag{13}$$

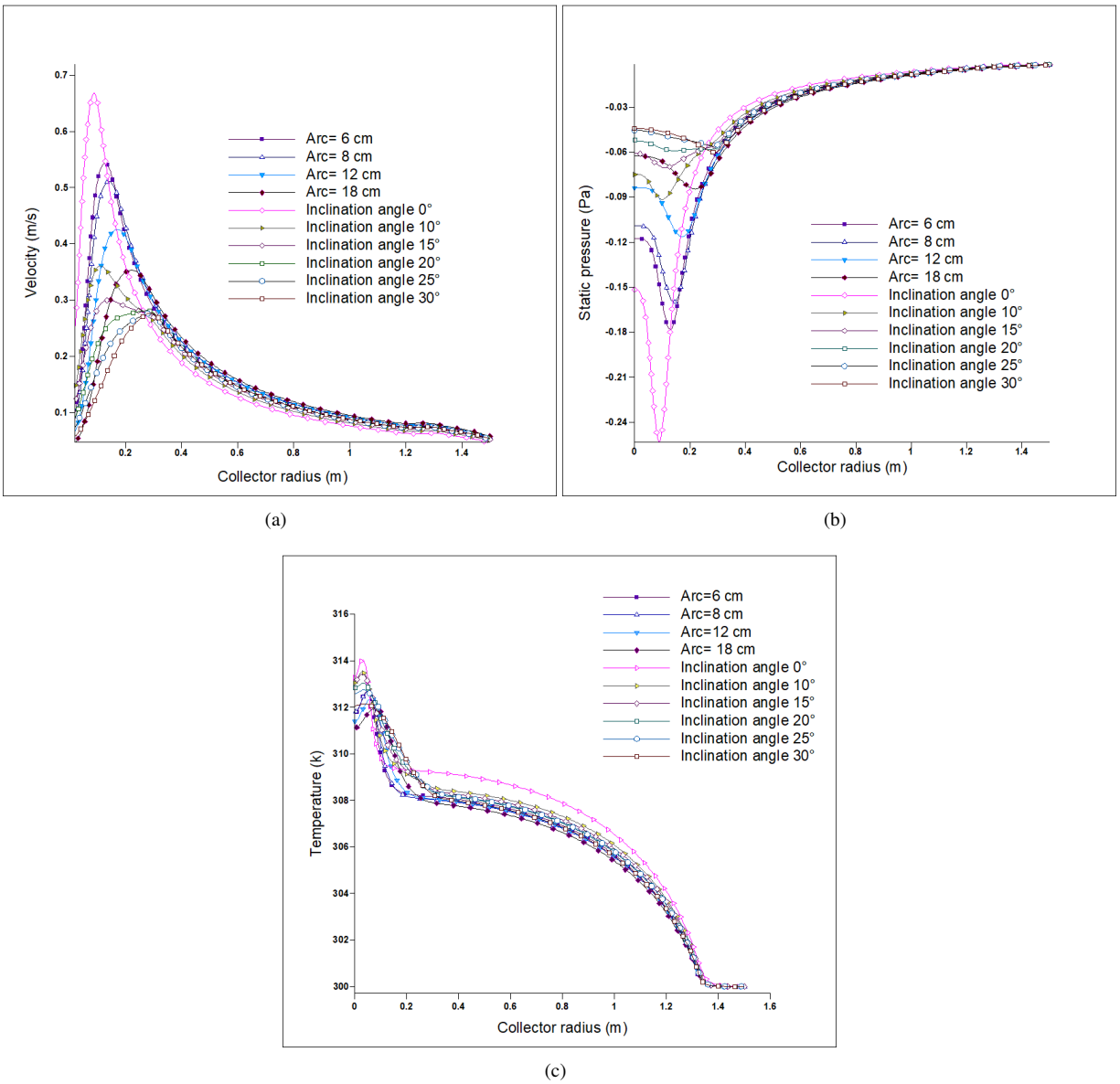

Figure 7. Effect of inclination angle and arc radius on the profile distributions of: (a) Velocity; (b) Static pressure; (c) Temperature in a solar chimney power plants (SCPP) with a conventional chimney base

3.1.2 Influence of geometry on pressure and temperature

Figure 8 illustrates the static pressure contours, indicates that the inclined collector (θ = 20°) presents sharp pressure gradients and localized losses at the chimney inlet, whereas the arc radius configuration (R_{Arc} = 18 cm) achieves a smoother pressure distribution with reduced drops. This improved pressure field enhances suction, leading to higher mass flow rates and increased power density. The static pressure distribution along the collector radius for different configurations is presented in Figure 7. Introducing an arc radius at the collector-chimney junction significantly enhances flow acceleration beneath the collector.The configuration with a 6 cm arc radius exhibits a pressure drop of -0.181 Pa, which is approximately 16.8 % higher in magnitude than that of the 10° inclined collector configuration (-0.155 Pa). However, when compared to the conventional chimney geometry (-1.834 Pa), this value

corresponds to a reduction in pressure losses of about 90 %. This significant decrease confirms that a smoother collector-chimney junction effectively reduces flow resistance and enhances momentum transport along the collector.

Figure 9 show that, although the optimized inclined collector configuration (θ = 20°) slightly improves the temperature distribution near the chimney base, pronounced thermal gradients persist at the collector-chimney junction. In contrast, the arc radius configuration (R_{Arc} = 18 cm) provides a smoother and more uniform thermal field, contributing to reduced local thermal gradients and improved aerodynamic conditions. As illustrated in Figure 7, the differences in outlet temperature among the investigated configurations remain limited. The conventional configuration (0°) reaches the highest outlet temperature of 314 K, which is only about 0.5 % higher than that of the 6 cm arc configuration (312.5 K) and slightly higher than the 10° inclined case (313.4 K, ≈ 0.3 %). These small variations indicate that geometric modifications primarily influence the aerodynamic performance of the system, while their impact on the overall thermal behavior remains marginal.

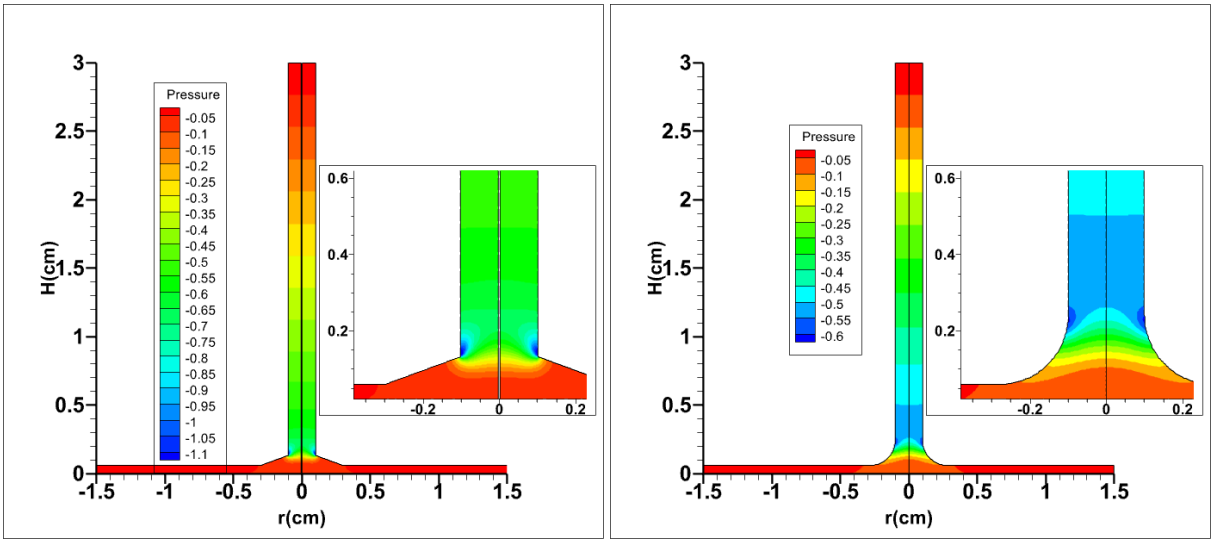

(a) Inclination angle θ = 20° (b) With an arc radius = 18 cm

Figure 8. Pressure contours for a solar chimney power plants (SCPP) with a conventional chimney base

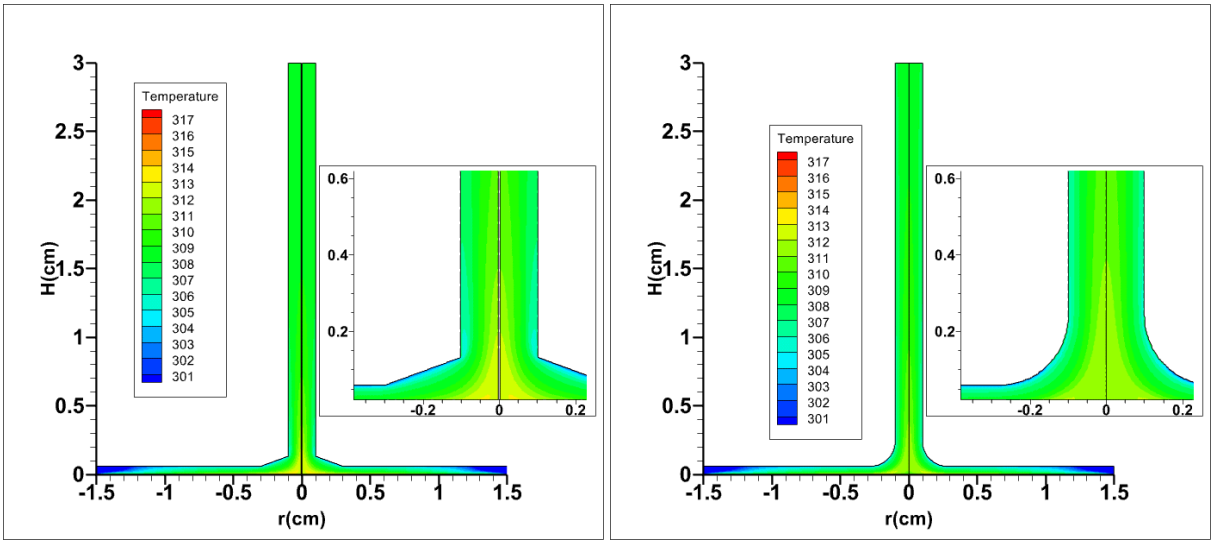

(a) Inclination angle θ = 20° (b) With an arc radius = 18 cm

Figure 9. Temperature contours for a solar chimney power plants (SCPP) with a conventional chimney base

3.2 The Effect of the Fillet Radius Variation on the Velocity and Pressure

In this section, the analysis is extended to examine the effect of fillet radius variations at the chimney base, considering values of 8 cm, 12 cm, and 14 cm, as illustrated in Figure 3. To ensure a consistent and systematic evaluation, the fillet radius is kept fixed for each set of simulations, while the effects of the arc radius and collector inclination angle are investigated. Figure 10 present the variations of these parameters for each fixed fillet radius. This stepwise approach enables a clear comparison among configurations and facilitates the identification of the best-performing geometry for the present study.

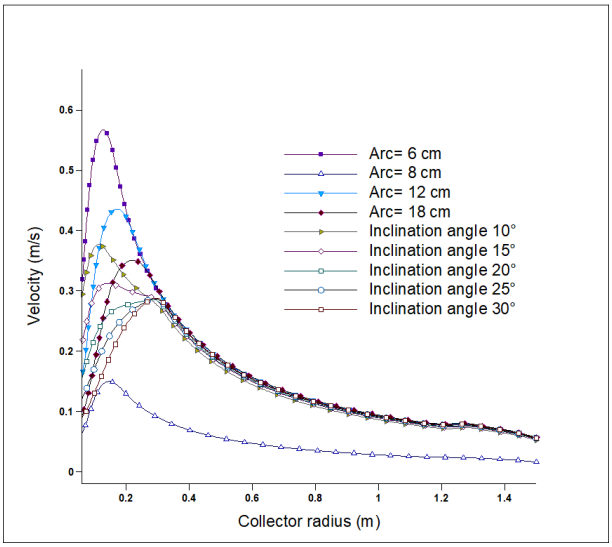

(a) Chimney base with fillet radius = 8 cm

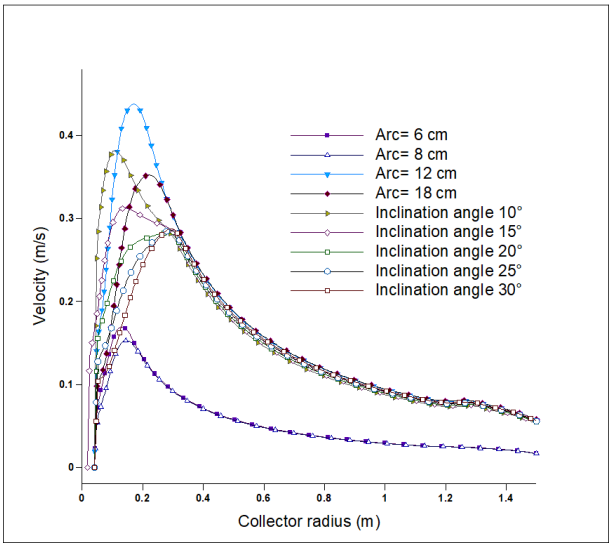

(b) Chimney base with fillet radius = 12 cm

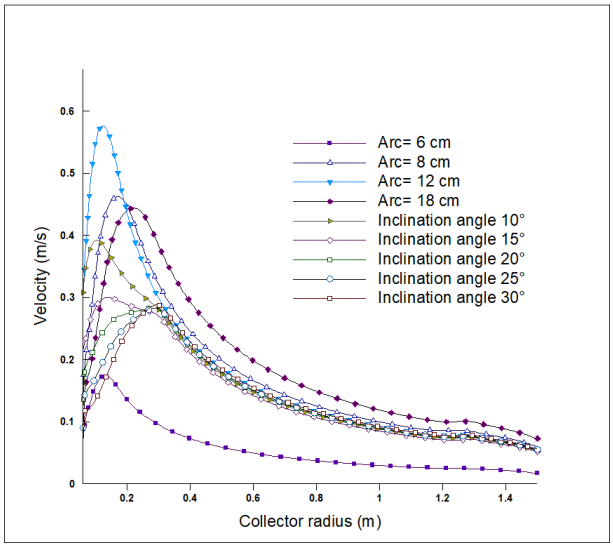

(c) Chimney base with fillet radius = 14 cm

Figure 10. Effect of inclination angle and arc radius on velocity profile distributions in a solar chimney power plants (SCPP) for different variation of chimney base with fillet radius

3.2.1 Influence on velocity

For all configurations, the air velocity increases rapidly near the collector center, reaches a maximum in the inner region ($r \approx 0.15$–0.30 m), and then gradually decreases toward the chimney.

By comparing Figure 10(a), (b), and (c), it is observed that increasing the chimney base fillet radius leads to a systematic increase in the maximum velocity. The velocity profiles become smoother and more stable, indicating a more efficient aerodynamic transition at the collector–chimney junction.

Since Figure 10(c) records the highest velocity values, the configuration with a fillet radius of 14 cm is selected as the reference case to evaluate the effects of the collector arc radius and collector inclination angle. It is clearly

observed that increasing the collector arc radius results in a progressive rise in the maximum velocity, along with more uniform and radially extended velocity profiles. In particular, the maximum velocity increases from 0.18 m/s for a collector arc radius of 6 cm to 0.57 m/s for an arc radius of 12 cm, corresponding to a percentage increase of 216.7%.

In contrast, variations in the collector inclination angle induce only limited changes in the airflow characteristics. The configuration with a 10° inclination exhibits the highest peak velocity, reaching approximately 0.39 m/s.

As the inclination angle increases from 10° to 30°, the peak velocity decreases and tends to stabilize for inclination angles of 20°, 25°, and 30°, with values of about 0.28 m/s. This behavior indicates that higher inclination angles do not significantly enhance flow acceleration and that, beyond moderate values, the influence of the inclination angle on the velocity field becomes marginal when compared to the effect of the collector arc radius.

Overall, the configuration combining a chimney base fillet radius of 14 cm with a collector arc radius of 12 cm achieves the highest airflow velocity, confirming that the collector inclination angle plays a secondary role compared to the fillet and arc radius in governing the aerodynamic performance of the solar chimney power plant. Consistent with the velocity contour distributions shown in Figure 11(a) and (b), the airflow within the collector exhibits low velocities near the inlet, followed by a gradual acceleration along the collector length and a pronounced acceleration region near the outlet.

The maximum velocity of 1.24 m/s observed for the 12 cm arc-radius configuration highlights the effectiveness of the optimized junction geometry in enhancing airflow characteristics.

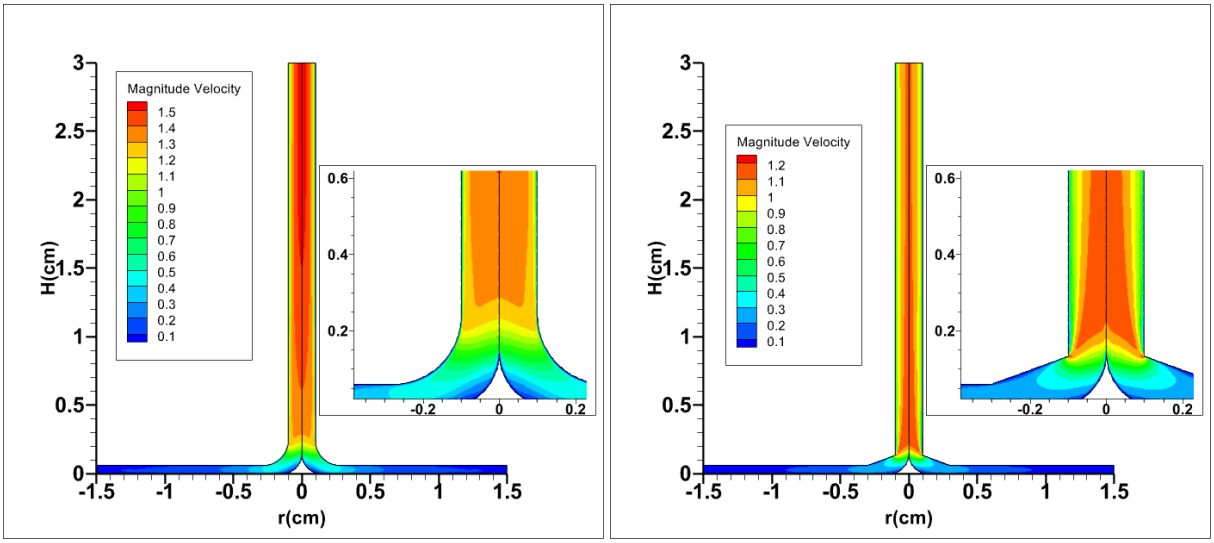

(a) With an arc radius = 12 cm

(b) With an inclination angle of 20°

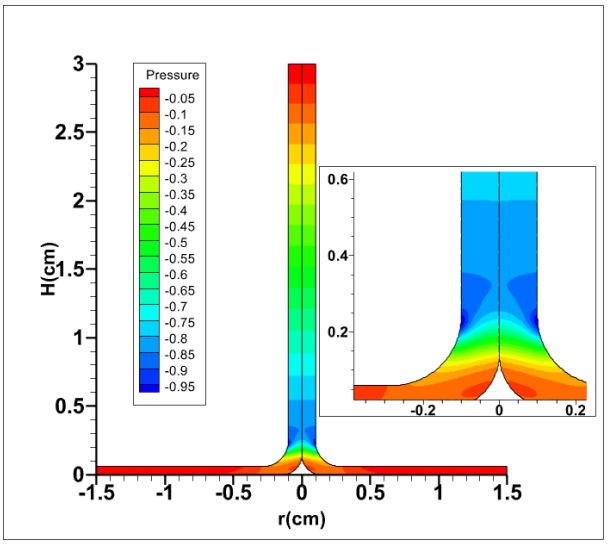

(c) With an arc radius = 12 cm

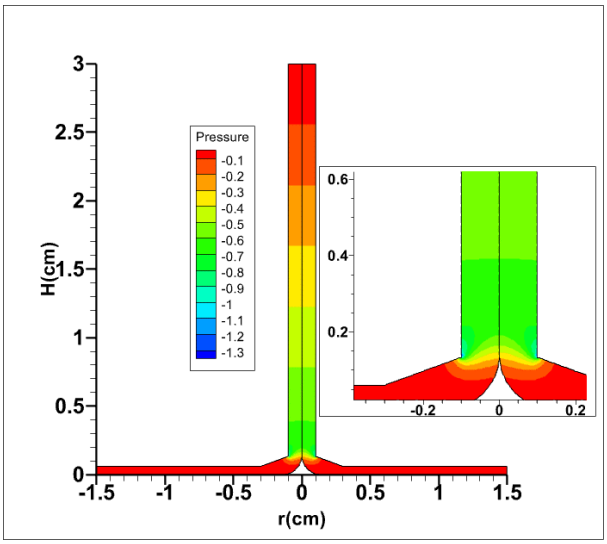

(d) With an inclination angle = 20°

Figure 11. Velocity contours for a fillet radius = 12 cm

3.2.2 Influence on pressure

Figure 12(a), (b), and (c) illustrate the effects of the collector inclination angle and arc radius on the static pressure distribution for different chimney base configurations with fillet radius of 8 cm, 12 cm, and 14 cm. The pressure drop within the chimney is mainly attributed to flow acceleration and losses caused by abrupt flow transitions [21]. Increasing the fillet radius clearly improves the static pressure distribution, indicating smoother flow paths and reduced local pressure losses at the collector-chimney junction.

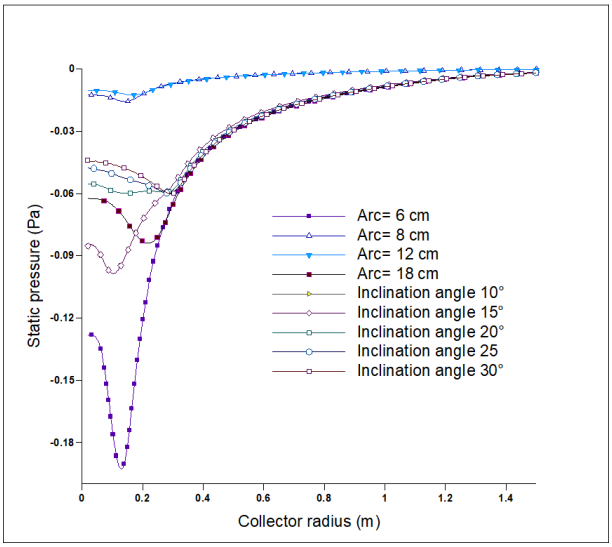

(a) Chimney base with fillet radius = 8 cm

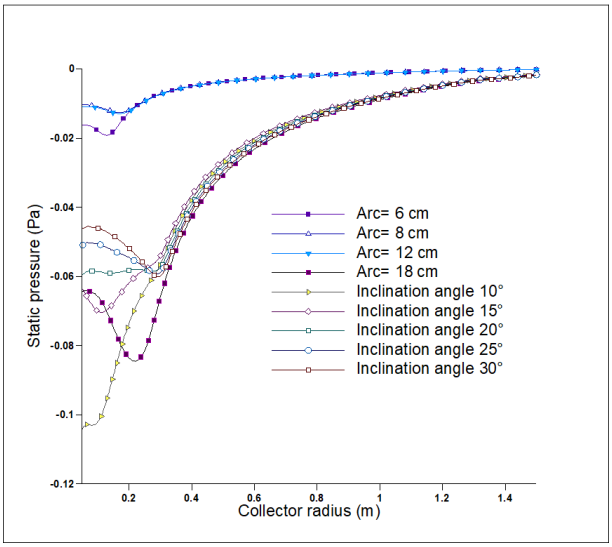

(b) Chimney base with fillet radius = 12 cm

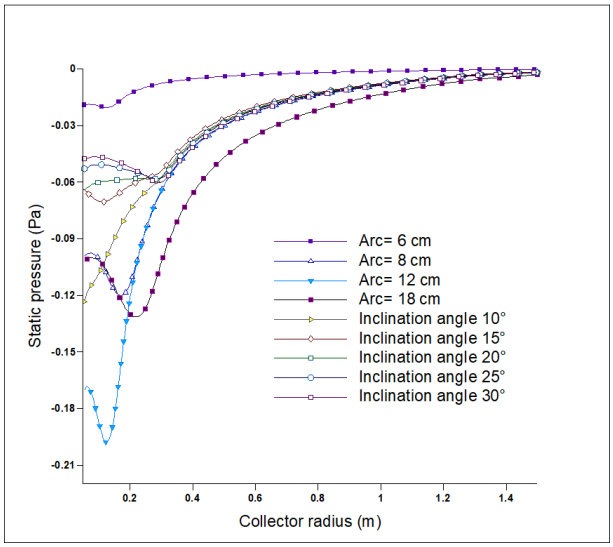

(c) Chimney base with fillet radius = 14 cm

Figure 12. Pressure profile distributions in a solar chimney power plants (SCPP) for different variation of chimney base with fillet radius

For a fillet radius of 8 cm, the pressure profile exhibits a pronounced negative peak near the collector center, with a minimum static pressure of approximately -0.17 Pa for an arc radius of 6 cm, indicating significant local pressure losses at the collector-chimney junction.

Increasing the fillet radius to 12 cm reduces the magnitude of the negative pressure to about -0.12 Pa and results in a smoother pressure gradient along the collector radius. For the largest fillet radius of 14 cm, the pressure distribution becomes more uniform and stable, with a minimum static pressure of approximately -0.19 Pa for an arc radius of 12 cm. Despite this local minimum, the overall pressure profile is smoother, suggesting reduced flow separation and improved aerodynamic behavior at the junction.

A comparison of the minimum pressure values for fillet radius of 8 cm (-0.17 Pa) and 12 cm (-0.12 Pa) reveals an approximate 29 % reduction in the maximum pressure drop. This result confirms that increasing the fillet radius

at the chimney base significantly improves aerodynamic performance by mitigating local pressure losses at the collector-chimney junction.

The comparison between arc-shaped geometries and inclined collector configurations, presented in Figure 12(c), is conducted by fixing a 14 cm fillet radius at the chimney base, as this configuration provides the smoothest and most uniform pressure profiles, indicating reduced local pressure losses. Arc configurations generate stronger depressions near the chimney inlet, with minimum pressure values of approximately -0.13 Pa and -0.19 Pa for arc radius of 18 cm and 12 cm, respectively, reflecting enhanced flow acceleration.

In contrast, inclined configurations exhibit more moderate pressure variations, with minimum values of about -0.07 Pa and -0.12 Pa for inclination angles of 15° and 10°, confirming that, for a large fillet radius, the use of an arc is more effective than inclination alone in improving the aerodynamic performance of the SCPP. These trends are further confirmed by the pressure fields shown in Figure 11(c) and (d).

3.3 Effect of Geometric Parameters on Mass Flow Rate and Power Output

Figure 13 and Figure 14 present the variation of the mass flow rate and the theoretical power density as functions of the fillet radius for different arc radii and collector inclination angles.

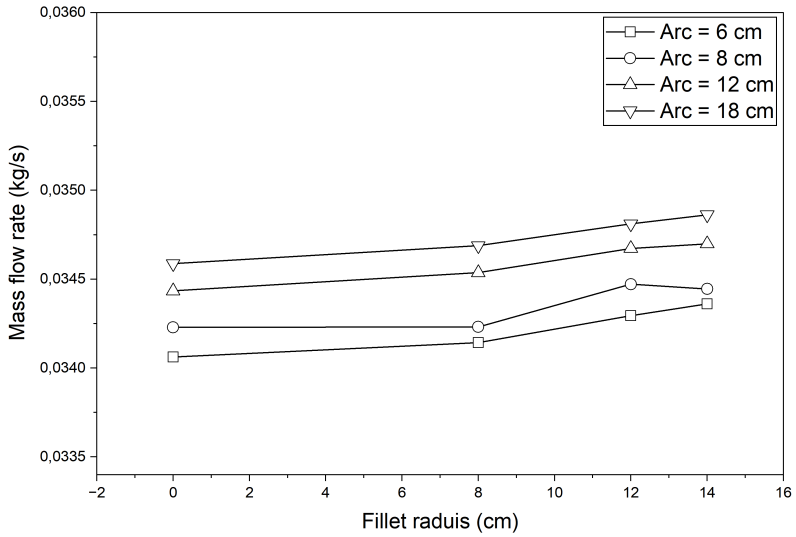

(a) Variation in arc radius

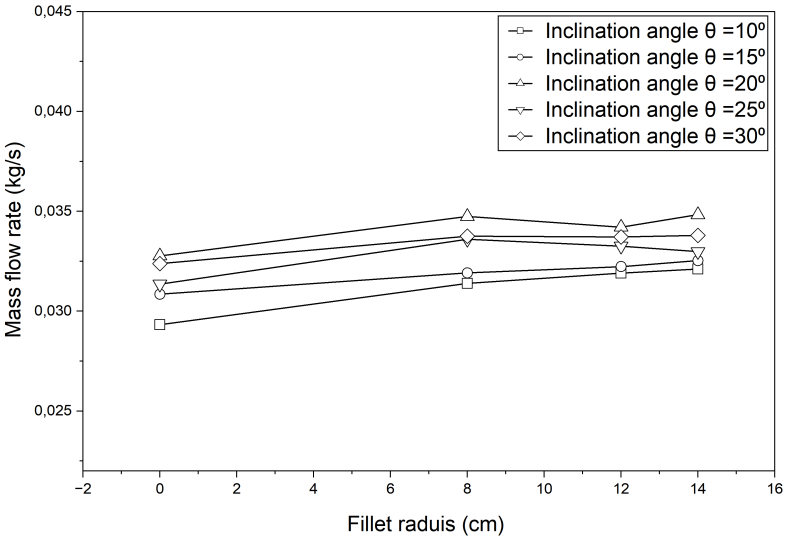

(b) Variation in inclination angle

Figure 13. Mass flow rate as a function for all fillet radius

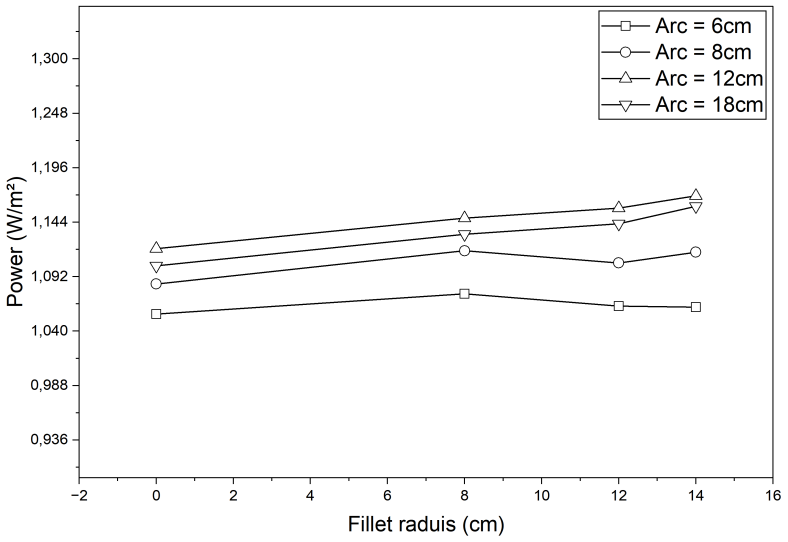

(a) Variation in arc radius

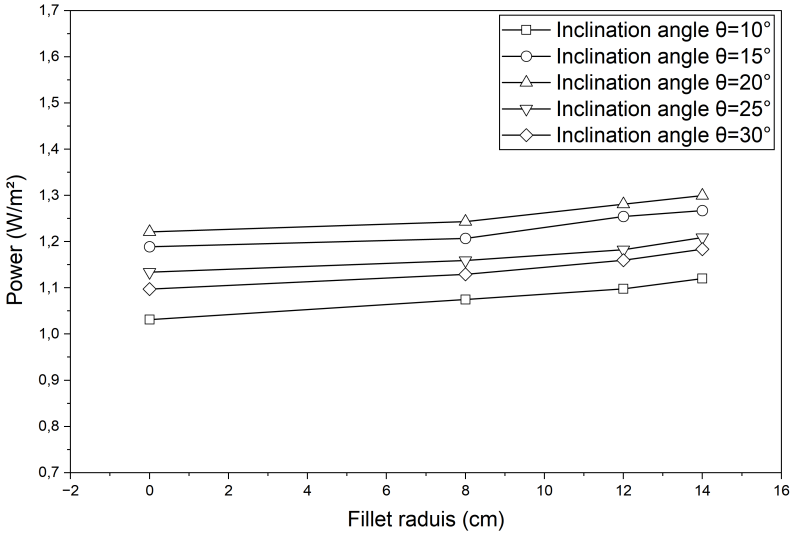

(b) Variation in inclination angle

Figure 14. Power as a function for all fillet radius

3.3.1 Effect of arc radius

Figure 13 illustrates the influence of the arc radius on the mass flow rate for various fillet radius. For all investigated cases, increasing the arc radius from 6 cm to 18 cm leads to a monotonic increase in the mass flow rate. For example, at a fillet radius of 14 cm, the mass flow rate increases from approximately 0.0343 kg/s for an arc radius of 6 cm to about 0.0349 kg/s for an arc radius of 18cm, corresponding to an improvement of nearly 1.7 %. This trend is consistently observed for smaller fillet radius, confirming that larger arc radius promote smoother flow guidance at the collector-chimney junction.

Moreover, the introduction of a fillet radius systematically enhances the mass flow rate compared to the corresponding configurations without a fillet. The optimal configuration among the arc radius cases is obtained for an 18 cm arc radius combined with a 14 cm fillet radius, which achieves a maximum mass flow rate of approximately 0.0349 kg/s, representing an improvement of about 8 % relative to the same arc-radius configuration without a fillet. This improvement can be attributed to reduced flow separation and lower aerodynamic losses at the chimney base.

The corresponding effect on the power density is shown in Figure 14. For a given fillet radius, increasing the arc radius from 6 cm to 18 cm results in a systematic increase in power density. At a fillet radius of 14 cm, the power

density rises from approximately 1.07 W/m^2 to about 1.15 W/m^2, corresponding to an improvement of nearly 7.5 %. This confirms that the aerodynamic enhancement induced by a larger arc radius directly translates into improved power output.

3.3.2 Effect of collector inclination angle

Figure 13 presents the variation of the mass flow rate with the collector inclination angle for different fillet radius. For a given fillet radius, increasing the inclination angle from 10° to 30° leads to a noticeable enhancement in the mass flow rate. At a fillet radius of 14 cm, the mass flow rate increases from approximately 0.0321 kg/s at 10° to about 0.0326 kg/s at 20°, corresponding to an improvement of nearly 1.5 %.

Consequently, the optimal inclination angle is identified as 20°, when combined with a 14 cm fillet radius, yielding the highest mass flow rate among all inclination angle cases. Compared to the same inclination angle without a fillet radius (0.0316 kg/s), this configuration exhibits an increase of approximately 3.2 %, highlighting the significant role of the fillet in improving flow smoothness and momentum transfer.

The influence of the collector inclination angle on the power density is depicted in Figure 14(b). For all fillet radius, the power density increases as the inclination angle rises from 10° to 20°. At a fillet radius of 14 cm, the power density increases from approximately 1.12 W/m^2 at 10° to about 1.29W/m^2 at 20°, corresponding to an improvement of nearly 15 %. Beyond this angle, the rate of improvement diminishes, confirming that excessive inclination adversely affects the aerodynamic performance.

4 Conclusions

This paper presented a numerical investigation of a SCPP to analyze the influence of the collector–chimney junction geometry on airflow and thermal performance. Using the standard k-ε turbulence model coupled with the DO radiation model, the study evaluated various geometric configurations under a constant solar irradiation of 850 W/m^2. Based on the simulation results, the following conclusions are drawn:

• Impact of Junction Geometry: The geometry of the collector chimney interface is critical for system performance. Introducing a curved junction (fillet) significantly suppresses flow recirculation zones and reduces pressure drops compared to the conventional sharp-edged design.

• Increasing the arc radius from 6 cm to 18 cm consistently enhances the mass flow rate and power density, with the most favorable performance achieved for an 18 cm arc combined with a 14 cm fillet radius. increases the mass flow rate by approximately 1.7 % and the power density by about 7.5 % compared to a smaller arc radius of 6 cm. The improvement is mainly attributed to smoother airflow and reduced aerodynamic losses at the collector-chimney junction.

• The optimal inclination of 20° combined with a 14 cm fillet radius results in an increase in mass flow rate of approximately 3.2 % and an improvement in power density of nearly 15 % compared to the same angle without fillet. due to smoother airflow transition and reduced friction losses at the junction. Deviations from this optimal angle, either higher or lower, lead to reduced performance due to less favorable flow acceleration and increased aerodynamic losses.

• The comparison between configurations with and without fillet radius reveals that introducing a rounded junction significantly enhances the performance. These results confirm that the curved transition contributes to smoother airflow and improved aerodynamic efficiency at the collector-chimney interface.

• Overall, the study confirms that geometric optimization of the collector-chimney interface is a simple yet effective strategy to enhance both aerodynamic and thermal efficiencies of SCPP, offering valuable insights for the design of future large-scale solar chimney systems.

Limitations and Future Work:

While this study demonstrates the benefits of geometric optimization, certain limitations must be acknowledged. First, the reliance on a 2D axisymmetric model assumes perfect flow symmetry and may not fully capture complex three-dimensional vortex shedding at the chimney inlet. Second, the simulations were conducted under constant solar irradiance, neglecting the transient thermal inertia effects caused by diurnal solar cycles. Finally, the model validation relied on small-scale experimental data. Future research will focus on full 3D transient simulations to account for environmental variations and will seek validation against larger-scale pilot facilities to ensure scalability of these findings.

Data Availability

The data used to support the research findings are available from the corresponding author upon request.

Conflicts of Interest

The authors declare no conflicts of interest.

References

[1] W. Haaf, K. Friedrich, G. Mayr, and J. Sclaich, "Solar chimneys part I: Principle and construction of the pilot plant in Manzanares," *Int. J. Sol. Energy*, vol. 2, no. 1, pp. 3–20, 1983. https://doi.org/10.1080/01425918308909911

[2] R. Rabehi, A. Chaker, Z. Aouachria, and M. Tingzhen, "CFD analysis on the performance of a solar chimney power plant system: Case study in Algeria," *Int. J. Green Energy*, vol. 14, no. 13, pp. 1081–1091, 2017. https://doi.org/10.1080/15435075.2017.1339043

[3] A. Sellami, D. Benlahcene, A. H. Benmachiche, and Z. Aouachria, "Performance analysis of a solar chimney power plant system in two Algeria regions," *Int. J. Ambient Energy*, vol. 43, no. 1, pp. 4820–4831, 2021. https://doi.org/10.1080/01430750.2021.1922500

[4] H. H. Al-Kayiem, A. M. Tukkee, A. Uddin, H. A. K. Shahad, and H. A. Abdul Wahhab, "Aerothermodynamics computational analysis of the collector of a hybrid solar chimney power plant integrated with a gas turbine power plant," *Int. J. Heat Technol.*, vol. 43, no. 4, pp. 1461–1473, 2025. https://doi.org/10.18280/ijht.430423

[5] A. Habibollahzadea, E. Houshfar, M. Ashjaee, A. Behzadi, E. Gholamian, and H. Mehdizadeh, "Enhanced power generation through integrated renewable energy plants: Solar chimney and waste-to-energy," *Energy Convers. Manag.*, vol. 174, pp. 875–888, 2018. https://doi.org/10.1016/j.enconman.2018.04.010

[6] A. P. Singh, A. Kumar, Akshayveer, and O. P. Singh, "Performance enhancement strategies of a hybrid solar chimney power plant integrated with photovoltaic panel," *Energy Convers. Manag.*, vol. 224, p. 113020, 2020. https://doi.org/10.1016/j.enconman.2020.113020

[7] M. Pandey, B. N. Padhi, and M. Ipsita, "Performance analysis of a waste heat recovery solar chimney for nocturnal use," *J. Energy Storage*, vol. 38, p. 102525, 2021. https://doi.org/10.1016/j.jestch.2020.11.009

[8] M. Mohammed, M. Jafari, F. Ranjbar, and L. Garousi Farshi, "Assessing the impact of cavity structure on collector and using PCMs on solar chimney power plant performance," *Int. J. Heat Technol.*, vol. 43, no. 2, pp. 721–730, 2025. https://doi.org/10.18280/ijht.430231

[9] A. Azad, E. Aghaei, A. Jalali, and P. Ahmadi, "Multi-objective optimization of a solar chimney for power generation and water desalination using neural network," *Energy Convers. Manag.*, vol. 239, p. 114152, 2021. https://doi.org/10.1016/j.enconman.2021.114152

[10] N. Fadaei, W. M. Yan, M. M. Tafarroj, and A. Kasaeian, "The application of artificial neural networks to predict the performance of solar chimney filled with phase change materials," *Energy Convers. Manag.*, vol. 171, pp. 1255–1262, 2018. https://doi.org/10.1016/j.enconman.2018.06.055

[11] D. K. Mandal, N. Biswas, and N. K. Manna, "An application of artificial neural network (ANN) for comparative performance assessment of solar chimney (SC) plant for green energy production," *Sci. Rep.*, vol. 14, p. 979, 2024. https://doi.org/10.1038/s41598-023-46505-1

[12] H. M. Abdul Hussein, N. A. Jabbar, and A. R. Zainy, "Flow modeling for hybrid solar chimney system optimization using nozzle and canopy," *Int. J. Heat Technol.*, vol. 43, no. 4, p. 432, 2025. https://doi.org/10.18280/ijht.430432

[13] E. Cuce, H. Sen, and P. M. Cuce, "Numerical performance modelling of solar chimney power plants: Influence of chimney height for a pilot plant in Manzanares, Spain," *Sustain. Energy Technol. Assess.*, vol. 40, p. 100704, 2020. https://doi.org/10.1016/j.seta.2020.100704

[14] P. M. Cuce, E. Cuce, D. K. Mandal, D. K. Gayen, M. Asif, A. Bouabidi, S. Alshahrani, C. Prakash, and M. E. M. Soudagar, "ANN and CFD-driven research on main performance characteristics of solar chimney power plants: Impact of chimney and collector angle," *Case Stud. Therm. Eng.*, vol. 50, p. 104568, 2024. https://doi.org/10.1016/j.csite.2024.104568

[15] B. Ghernaout, S. Bouabdallah, M. E. H. Attia, M. Arici, and Z. Driss, "Parametric study of the airflow structure in a solar chimney," *Int. J. Heat Technol.*, vol. 38, no. 2, pp. 285–292, 2020. https://doi.org/10.18280/ijht.380202

[16] A. Kasaeian, M. Ghalamchi, and M. Ghalamchi, "Simulation and optimization of geometric parameters of a solar chimney in Tehran," *Energy Convers. Manag.*, vol. 78, pp. 107–111, 2014. https://doi.org/10.1016/j.enconman.2014.03.042

[17] M. Ghalamchi, A. Kasaeian, M. Ghalamchi, and A. H. Mirzahosseini, "An experimental study on the thermal performance of a solar chimney with different dimensional parameters," *Renew. Energy*, vol. 91, pp. 477–483, 2016. https://doi.org/10.1016/j.renene.2016.01.091

[18] D. K. Mandal, N. Biswas, A. Barman, R. Chakraborty, and N. K. Manna, "A novel design of absorber surface of solar chimney power plant (SCPP): Thermal assessment, exergy and regression analysis," *Sustain. Energy Technol. Assess.*, vol. 56, p. 103039, 2023. https://doi.org/10.1016/j.seta.2023.103039

[19] A. P. Singh, A. Kumar, Akshayveer, and O. P. Singh, "A novel concept of integrating bell-mouth inlet in converging-diverging solar chimney power plant," *Renew. Energy*, vol. 169, pp. 318–334, 2021. https://doi.or

g/10.1016/j.renene.2020.12.120

[20] D. K. Mandal, N. Biswas, and N. K. Manna, "An application of artificial neural network (ANN) for comparative performance assessment of solar chimney (SC) plant for green energy production," *Sci. Rep.*, vol. 14, p. 979, 2024. https://doi.org/10.1038/s41598-023-46505-1

[21] T. Singh and A. Kumar, "Numerical analysis of the divergent solar chimney power plant with a novel arc and fillet radius at the chimney base region," *Renew. Energy*, vol. 224, p. 120504, 2024. https://doi.org/10.1016/j.renene.2024.120504

[22] J. C. Pretorius and D. G. Kroger, "Critical evaluation of solar chimney power plant performance," *Sol. Energy*, vol. 80, no. 5, pp. 535–544, 2006. https://doi.org/10.1016/j.solener.2005.04.001

[23] M. Kaplan, "Influence of inclination angle at the chimney inlet on the power generation in solar chimney power plants through 3D CFD model," *Int. J. Photoenergy*, vol. 2023, p. 7394007, 2023. https://doi.org/10.1155/2023/7394007

[24] A. Mirzamohammad, M. Eftekhari Yazdi, and A. M. Lavasani, "Improvement of combined solar chimney power plant with gas power plant," *Sci. Rep.*, vol. 13, p. 11220, 2023. https://doi.org/10.1038/s41598-023-38464-4

[25] M. Rahimi-Larki, A. Arefian, S. Nazari, A. Torkfar, R. Hosseini-Abardeh, and H. Sarlak, "Performance investigation of a sloped collector solar chimney system exposed to the ambient crosswind," *Energy*, vol. 318, p. 134732, 2025. https://doi.org/10.1016/j.energy.2025.134732

[26] A. Ayadi, H. Nasraoui, A. Bouabidi, Z. Driss, M. Bsisa, and M. S. Abid, "Effect of the turbulence model on the simulation of the air flow in a solar chimney," *Int. J. Therm. Sci.*, vol. 130, pp. 423–434, 2018. https://doi.org/10.1016/j.ijthermalsci.2018.04.038

[27] O. A. Najm and S. Shaaban, "Numerical investigation and optimization of the solar chimney collector performance and power density," *Energy Convers. Manag.*, vol. 168, pp. 515–528, 2018. https://doi.org/10.1016/j.enconman.2018.04.089

[28] D. Toghraie, A. Karami, M. Afrand, and A. Karimipour, "Effects of geometric parameters on the performance of solar chimney power plants," *Energy*, vol. 162, pp. 1052–1061, 2018. https://doi.org/10.1016/j.energy.2018.08.086

[29] H. Nasraoui, M. Bsisa, and Z. Driss, *Solar Chimney Power Plants: Numerical Investigations and Experimental Validation*. Bentham Science Publishers, 2020. https://doi.org/10.2174/9789811461750120040 1

[30] J. Schlaich, R. Bergermann, W. Schiel, and G. Weinrebe, "Design of commercial solar updraft tower systems—Utilization of solar induced convective flows for power generation," *J. Sol. Energy Eng.*, vol. 127, no. 1, pp. 117–124, 2005. https://doi.org/10.1115/1.1823493

[31] E. Özgirgin Yapici, E. Ayli, and O. Nsaif, "Numerical investigation on the performance of a small scale solar chimney power plant for different geometrical parameters," *J. Clean. Prod.*, vol. 276, p. 122908, 2020. https://doi.org/10.1016/j.jclepro.2020.122908

[32] E. M. Abo-Zahhad, A. A. Hachicha, M. Z. Mistarihi, M. H. Salim, and M. F. C. Esmail, "Optimization of ground material properties for enhanced solar chimney power plant efficiency: A CFD and RSM approach," *Energy Rep.*, vol. 13, pp. 3929–3945, 2025. https://doi.org/10.1016/j.egyr.2025.03.035

Nomenclature

$A_{chimney}$	Chimney area, m^2
c_p	Specific heat of air, kJ/kg K
C_1, C_2	Constants for the turbulence model
D_{coll}	Collector diameter, m
$D_{chimney}$	Chimney diameter, m
g	Acceleration due to gravity, $\mathrm{m/s}^2$
$H_{chimney}$	Chimney height, m
I	Solar irradiation, W/m^2
$\dot{m}$	Mass flow rate, kg/s
P	Theoretical power produced, $\mathrm{w/m}^2$
P_{tot}	Power output, W
R_{Arc}	Arc radius, cm
R_{fillet}	Fillet radius, cm
T_a	Ambient temperature, K
v	Maximum air velocity, m/s
x	Horizontal coordinate, m
y	Vertical coordinate, m

Greek symbols

β	Thermal expansion coefficient
μ	Dynamic viscosity of air, Ns/m^2
$\eta_{chimney}$	Chimney efficiency, %
ρ	Ambient air density, kg/m^3
θ_{Coll}	Inclination angle, $^\circ$